University of Texas Rio Grande Valley

ScholarWorks @ UTRGV

8-2020

Nonwovens of Ceramic Decorated Cellulose Based Fine Fibers for Leaded Water Purification

Alejandro J. Castillo
The University of Texas Rio Grande Valley

NONWOVENS OF CERAMIC DECORATED CELLULOSE BASED FINE FIBERS FOR

LEADED WATER PURIFICATION

A Thesis

by

ALEJANDRO J CASTILLO

Submitted to the Graduate College of
The University of Texas Rio Grande Valley
In partial fulfillment of the requirement for the degree of:

MASTER OF SCIENCE

AUGUST 2020

Major Subject: CHEMISTRY

NONWOVENS OF CERAMIC DECORATED CELLULOSE BASED FINE FIBERS FOR

LEADED WATER PURIFICATION

A Thesis
by
ALEJANDRO J CASTILLO

Committee Members

Dr. Karen Lozano ,
Co-chair of committee

Dr. Mohammad Jasim Uddin
Co-Chair of committee

Dr. Karen Martirosyan
Committee member

AUGUST 2020

ABSTRACT

Castillo, Alejandro J. <u>Nonwovens of Ceramic Decorated Cellulose Based Fine Fibers for Leaded Water Purification</u>. Master of Science (MS), August 2020, 55 pp, 1 table, 17 figures, 67 titled references

Fine fibers of cellulose acetate were Forcespun and used to make nonwoven mats of cellulose. Nonwovens were activated using a solution combustion synthesis which deposited iron nitride onto fibers. Cellulose and cellulose composite mats were tested as adsorbents for lead ion in water. Cellulose showed slightly higher adsorption capacities (mg/g) up to 1300 mg/g lead loading. Adsorption data were further analyzed using several isotherms, of which the Dubinin-Raduskevich gave the best fits.

ACKNOWLEDGMENT

TABLE OF CONTENTS

LIST OF TABLES

LIST OF FIGURES

CHAPTER I

INTRODUCTION

Philosophy of science as a profession

In order create 'impactful science' a researcher must fulfill the two tasks implied by the two words. Firstly, it must reveal something previously unrealized. This is where relationships are discovered, and innovations come to the state-of-the-art. Secondly, it must contribute the improvement of the quality of life for society and/or individuals. This is where problems like dirty water and energy are solved.

It is in technology where science and impact are most closely coupled. Through history, advancement in human well-being has been intimately connected with advancement to technology. However, it is well known that advances in consumer technology trail behind advances in technological capability, which themselves trail behind advances in science. Currently existing technology, like nuclear fusion, are unable to have an impact because they cannot be implemented at scale, either because necessary techniques are physically not scalable, or because it would be economically unviable to scale or use them. Once scalable, cost remains a limiting factor, with low cost technologies disseminating to the largest amount of people.

The responsibility of professional science lies not just in the advancement of understanding, but in the translation of that understanding into human advancement through the production of commercially viable technologies

Overall goals and objectives

Coming into vogue is the idea of wearable electronics. Early iterations of this idea relied on sewing small versions of available electronics into cloths. This has taken the form of things like LEDs for simple grid displays. As research has progressed, projects have arisen into making the textiles themselves reactive. This has included weaves with thermally expanding pores, fabric antennae patches, and a range of organic and inorganic inks. There has been some commercialization of organic semiconductor inks on commercial fabrics to make piezoelectric and conductometric devices to monitor cardiovascular indicators for the US military.

On the cutting-bleeding-edge of both device fabrication and wearable electronics is the fiber device architecture, wherein complete (or nearly complete) devices are incorporated into/onto a single fiber, usually inorganic. Prototype devices of this type include: dye sensitized solar cells, batteries, capacitors, and sensors. While certainly impressive as technology, the fabrication procedures are involved, expensive, and many-stepped. This presents significant obstacles to the upscaling of fabrication. Further, the weaving of individual fiber devices into an all-device textile is currently outside of our capabilities, and would be prohibitively expensive for mass production if it wasn't. Therefore, even as the capabilities of fiber devices continue to improve, technology which incorporates them remain out of reach.

Rather than creating individual fiber devices which are then woven into a textile, there is the equally intriguing possibility that fibers can be formed into a textile, and that a process performed on the textile can then form devices on all individual fibers. By developing a fiber device fabrication technique based in solution processing, it can be applied to every fiber in a textile. By also keeping reaction temperatures under the temperature at which polymer fibers degrade, the fabrication of devices on fibers can be simply inserted into the current textile

2

manufacturing infrastructure to produce advanced electronic fabrics at commercially viable volumes and cost.

This is a difficult and complicated goal. To maximize the relation between effort and progress, this goal is broken into graduated synthesis objectives, each of which is tied closely with an application of high societal impact. Each objective will build the techniques necessary for the next. These objectives and applications are as follows, in the order of their graduation:

1) the synthesis of simple oxide shells on cellulose fibers without pyrolysis and their use as adsorption membranes for the point-of-use remediation of leaded water

2) the addition of non-oxygen anions to the ceramic and the control of cellulose pyrolysis, including the graphitization of cellulose to act as fiber membrane electrodes in flexible batteries

3) the synthesis of complex oxide (multimetal or mutlilayer) shells on cellulose fibers of controlled pyrolysis for the fabrication of next generation energy harvesting devices

This thesis covers the aims, activities and results of the first objective. Technical nonwovens are used for the remediation of water. By focusing on a novel method for the decoration of fibers -while improving manufacturing metrics like activity, cost, volume, and time- we add value into a critical health issue while building the basic competencies of the solution combustion technique based decoration that will allow the fabrication of increasingly advanced fiber-level textile devices.

We make cellulose nonwoven mats from the mass production of cellulose acetate fibers, use a solution combustion synthesis to coat these nonwoven cellulose fibers with simple oxides of iron, nickel, and zinc, and test their lead adsorption characteristics at conditions important to the remediation of leaded tap water in urban household

3

CHAPTER II

LITERATURE REVIEW

Lead

In the body lead, like other heavy metals, disrupts cellular function, negatively affects

organ function, and targets the brain impairing cognition[1]. Due to this, lead is tied in with

every social ill, with studies reporting close coupling between blood lead levels (BLL**s**) and

statistical indicators like violent crime and disability[2-4]. Federal efforts to eliminate heavy

metal threats to public health have been expressed in the Environmental Protection Agency

(EPA)'s "Lead and Copper Rule", which currently sets federal action levels of 15ppb and

1.3ppm for lead and copper in potable water [5]. This means that above 15 ppb lead in water,

utility providers are federally mandated to take substantive action to redress lead levels. Since

the creation of this rule, surveillance of BLL**s** of children and adults have shown continually

falling levels through combined efforts to remove lead from gasoline, building materials, and

water [6-8].

This progress, from ~400 to <40 BLL**s**, is fantastic. However, any amount of lead in the

body, even 1 BLL**s**, has been proven to cause negative health outcomes [1]. High profile leaded

water crises, like Flint, MI, the DC Water Crisis and the current Pennsylvania Water Crisis have

focused attention onto the issue of pure water, resulting in coming reductions to the federal

4

action limit [7-11]. To continue to reduce heavy metal impact, advancement of metal-ion purification technology is required.

Review of literature covering leaded water incidents in the US, China, Europe, and Africa have concluded that that the primary avenue of lead introduction into potable water in non-industrial urban environments is via lead tainted pipes, leaded solder, and lead tainted pipe fittings, with specific tainted fittings sometimes being identified [11-18]. The oft cited causes of lead inclusion to metal working, even at this late date, are its cheapness and workability, with many brass fittings (in the US) allowed up to 8% weight lead in their alloy by law, until 2014.

While there are efforts to replace or coat pipes, much of the remaining leaded infrastructure is on the side of the homeowner and estimates by the Pennsylvania department of Environmental Protection put the cost of remediation at between 8,000-30,000 USD per site [12]. As well, efforts are sometimes complicated by confusion on the part of both private water utilities and government agencies [18, 19]. This situation is untenable and until costly upgrades to basic infrastructure are completed at an indeterminate time, a stop-gap measure in the form of private option for point-of-use water remediation is needed. Considering ease of use and cost restraints for maximum dissemination, the foremost effect to use is surface-adsorption of metal ions onto a substrate of maximum activity and minimum cost.

Adsorption

Surface adsorption is the process wherein a species in solution sticks to the surface of a material, or 'adsorbent'. This adherence can be traced to physical or chemical causes, separating adsorption into physi-sorption and chemi-sorption, respectively. In physi-sorption, favorable conditions like temperature or surface polarity cause a species to concentrate at the surface of an

adsorber, like in the case of condensation of water on a glass, or the adsorption of hydrogen onto graphene. In chemi-sorption, there is an exchange of electrons between the species and the surface, which results in chemical bond, sometimes called surface chelation. Physi-sorption is reversible, and is more suited to applications like hydrogen storage. Chemi-sorption requires an acid wash to free all metals from the surface, and is passive rather than active, making it more suitable for heavy metal purification. In the chemisorption of metals, positively charged metal cations in solution bond with negatively charged surface specie. These surface species are usually oxygen based, though they can be based in sulfur, or nitrogen. This addition of a positive ion to the surface necessitates the ejection of a positive ion from the surface to ensure charge neutrality, and this new oxygen-metal bond often replaces an oxygen-hydrogen bond, releasing hydrogen into solution.

The adsorption of species onto a surface can be described by numerous expressions, with varying levels of theory and different assumptions behind them. Here, we cover three isotherms: Freundlich, Langmuir, and Dubinin-Radushkevich, which were all originally formulated for the adsorption of gaseous species onto solid surfaces

The Langmuir equation has the most theoretical backing, in that it is derived from theory and not from fitting. It makes several assumptions about the nature of active sites in order to describe adsorption. These are that

- active sites are distinct

- active sites are equivalent

- adsorbed molecules do not interact with each other,

- adsorbed molecules only form a single layer on the surface

and it's expression takes the form

$$\theta = \frac{k_L Ce}{1 + KCe}$$

Where Θ is the fraction of species adsorbed, k s the Langmuir constant (mg/g) which is related to the adsorption capacity, and Ce which is the equilibrium concentration after adsorption.

The Freundlich equation is empirical, and there is the assumption that active sites are not equivalent, but rather have a Gaussian distribution of 'heats of adsorption'. Though there is less theoretical basis, this equation has two fitting parameters (K and n) and often fits data better as a result. This expression takes the form:

$$q_e = KCe^{1/n}$$

Where qe is the mass of adsorbent over mass adsorbate (loading capacity), K and n are fitting constants, and Ce is the equilibrium concentration.

The Dubinin-Radushkevic equation is semi-empirical and is used to examine microporous materials in the moderately dilute range. This equation takes the form:

$$q_e = Q_{DR}\exp(-k_{DR}[RT ln\left(1 + \frac{1}{Ce}\right)]^2)$$

Where Q and k are Dubinin-Radushkevic constants, R is the gas constant (in kJ/nK), and T is adsorption temperature.

Often, linearized forms of these equations are used. This entails the separation of terms via logarithms and the plotting of terms against one another to extract information about the remaining terms from the slope and intercept values via the equation of a line (y=mx+b). The

logarithm-separated expressions for the Langmuir, Freundlich, and Dubinin-Radushkevic

expressions are, respectively: (20-22)

$$\frac{Ce}{qe} = \frac{1}{q_{max}K_L} + \frac{qe}{qmax}$$

$$\ln(qe) = \ln(Kf) + \frac{1}{n}\ln(Ce)$$

$$\ln(qe) = \ln(qm) - [RTln(q + \frac{1}{Ce})]^2$$

Surface adsorption is often used in metal remediation. There has much work done in the

field of water filtration/purification polymer membranes. Adsorption membranes are often in a

nonwoven mat morphology. The reported work on these nonwovens have been mostly on fiber

membranes produced via the electrospinning process [22-27]. Activated nonwovens can show

high adsorption capacities, but the surface modification step adds enough cost that it is untenable

to commercialize into cheap water purification technologies. As well, the electrospinning process

requires high voltages, and is known to produce only lab-scale masses of nanofibers. For these

reasons, the electrospinning technique cannot (in most cases) be used to produce materials for

commercial applications. Polymers used are usually activated through chemical modification or

inorganic incorporation to increase the adsorptivity and/or selectivity of the membrane for metal

ions [23-28]. These substrate polymers often include cellulosics, which have a history of use in

environmental remediation.

Because volumes are so large in the environmental regime, cost of adsorbent has to be

very low, leading to much work being done on the adsorptive properties of materials based in

plant waste. This includes coffee grounds, sugar cane bagasse, algae of different types, coconut husks, rice husks, and so on [29-35]. Two common themes amongst them are that the adsorption sites are cellulosic in nature (meaning cellulose, hemicellulose, and chitin) and that the low-cost/renewable nature of their feedstock is highlighted.

Metal oxide nanoparticles have also featured heavily in remediation of heavy metal waters[36-41]. This is due to the exposed oxygen ions on the surface of oxides, some of which have dangling bonds. Simple oxides, including different iron oxide phases, zinc oxide, and manganese oxide, have shown good adsorptivity for heavy metals in aqueous solutions [36-41]. Likewise layered silicate clays like kaolinite and montmorillonite have also been used to remediate metallic waters with their hierarchical structures and naturally occurring sources making them attractive. Drawbacks of using ceramic powders, and to a lesser extent vegetable roughage, are that they are difficult/costly to recover from solution once dispersed, and that tight packing of particles leads to large pressure drops across packed filters.

Activated carbons are also a class of heavy metal adsorber, and many of the commercial products for metal adsorption seem to rely on carbon. Pure carbon is hydrophobic. To induce hydrophilicity, high temperature (>800*C) thermal or moderate temperature(~200*C) thermochemical treatments are used to introduce functional groups of oxygen to the surface [42-44]. This treatment should also induce porosity and high surface area into the material. This coupling of surface functionalization and increasing of surface area is the 'activation' step of creating activated carbon. While activated carbon materials are effective adsorbers, the high temperatures and chemical reagents are costly, and in the case of chemical activation produces liquid waste streams.

Common threads amongst regimes are the limiting nature of cost, and the constant pressure to reduce waste and resource use to produce materials. By dramatically reducing the liquid waste and energy cost of substrate activation, activating with cheap and earth abundant elements, and increasing the amount of produced materials by orders of magnitude, without sacrificing adsorption capacity, the next generation of heavy metal adsorption materials can be synthesized to meet worldwide demand for the total adsorption of heavy metals from water.

The characterization of adsorption materials is accomplished most simply by testing the concentration of a solution before and after contact with the adsorption material. This contact can be accomplished in the batch method, wherein a volume of liquid is enclosed with the adsorption material at given parameters, before filtering. This contact can also be accomplished in the column method, wherein a solution is passed through an adsorption material. While the column method produces data that's more directly useful for fabricating a filter, the batch method is much simpler while still being suitable for investigating materials and comparing them. This has resulted in the batch method predominating in the literature.

Depending on the concentration of metal ions tested, different methods can be used to determine their concentration. Copper is suitable for UV/Vis at ppm concentrations, while lead requires GFAA or ICP, especially at the low ppb concentrations of interest (100-0ppb).

Experimental parameters affecting the adsorption capacity (mg/kg) of metals onto substrates are: temperature, time, concentration, pH, and adsorbent:solution ratio. Material factors affecting adsorption are surface area, solvophilicity, and strength of the functional group – metal ion interaction

Combustion Synthesis

Ceramic materials are deposited in a combustion reaction of molecule and salt precursors (metal, ammonium, nitrate, chloride, urea, and others) loaded via aqueous solutions to cellulose surfaces.

This technique is based in the general class of redox reactions termed Self-propagating High-temperature Synthesis (SHS) reactions, or solid flame synthesis. Originally based on reactions between elemental powders, the first SHS syntheses took advantage of differences in reduction potentials between metals, oxides and metalloids to drive the synthesis of materials, rather than high *applied* temperatures. Once initiated at moderate temperatures, reduction-oxidation reactions (loss and gain of electrons, or changes in an elements *oxidation state*) can be exothermic enough to raise reaction temperatures well past ignition into the thousands of degrees Celsius.

In the first reactions, precursor powders were pressed into pellets or other monoliths, preheated, and ignited with some applied source of high heat. The reaction proceeds as a wave-front through the solid phase, with the waveform being broken into several zone, including the pre-reaction zone (where the reaction raises temperatures in the local vicinity, possibly changing phase), the reaction front (where electrons are exchanged, releasing energy and pushing ions into their most excited states), and the cooling region (where heat and mass transfer parameters control the final phase of products) [45]. This has been used to make many different materials, including oxides, nitrides, boronitrides, alloys, and sulfides, in morphologies ranging from monoliths, to powders, and coatings. This reaction happens very quickly, quicker than heat transfer coefficients/heat capacities of many materials. Because of this, it is conceptualized that heat produced by the reaction (Q) cannot escape the system in the time scale of the reaction. This

11

effectively makes it an adiabatic system, and it is assumed that the local reaction reaches a maximum adiabatic temperature (T_{ad}) before cooling begins.

A typical reaction is shown below (Eq.1)

$$ZrO_2 + B_2O_3 + 5Mg \rightarrow ZrB_2 + 5MgO \quad T_{ad} = 2100K$$

Note the adiabatic temperature reached from the exothermic heat of reaction is above 1500*C, that boron and magnesium are oxidizer and reductant respectively, and that all products are solid.

Since its inception and initial study, the **SHS** class of reaction has been used as the basis of several derivative techniques, including carbon combustion reactions and solution combustion reactions. In carbon combustion, reduction-oxidation between carbon and atmospheric oxygen is used to produce carbon dioxide and heat[46]. This does not form the products via the combustion itself, but rather uses the combustion heat to drive a separate material forming reaction.

In solution combustion, the typical reagents change. The oxidizer shifts from an elemental metal of zero (0) oxidation state, to the nitrate ions of metal nitrate salts. The fuel changes from inorganic precursors to organic molecules, usually urea or acetylacetonate, but also citric acid, glycine, and many other organic fuels [47].

This technique is often used with water as solvent, though organic solvents like 2-methoxyethanol are also used, especially when fabricating semiconductor films for solid-state devices. A typical solution combustion reaction is shown below (Eq. 2).

$$3Zn(NO_3)_2 \cdot 6H_2O + 5CH_4N_2O \rightarrow 3ZnO(s) + 8N_2(g) + 5CO_2(g) + 28H_2O(g)$$

Note that its products are the target ceramic (ZnO) and combustion gases (showing an absence of liquid waste streams), and that the calculated adiabatic temperature resultant from the exothermic heat release is below 800*C, but well in excess of polymer degradation temperatures.

This technique was first reported by Patil and Kinglsy in 1988, who used solutions of metal nitrates and urea to form aluminum oxide (and derivative) powders in a muffle furnace preheated to 500*C [48]. Since then, the solution combustion technique has been used to produce metallic and ceramic nanomaterials [49].

Almost invariably, syntheses use metal nitrate salts to provide both hydrated metal ions $[M(OH_2)_m,]^{m+}$ and oxidizing nitrate $(NO_3)^-$ species. Organic molecules are then added, which chelate the metal in a complex $[ML_x]^{m-l}$ that should be very soluble in the solvent of choice. Some of the common molecules used are citric acid/citrate, urea, acetylacetone/acetonate, glycine, and hydrazine. This precursor solution is then heated to drive off the solvent, and bring precursors to their reaction temperature. The solution increases in concentration and viscosity until the critical temperature (T_{ign}) is reached, and the ligands and nitrate ions begin their exothermic combustion. As this exothermic heat release is in intimate contact with metal ions over very fast time scales, freed metal ions reach adiabatic temperatures high enough that they cool into oxide (or otherwise desirable) phases as reaction products off-gas.

This ignition temperature marks different mechanisms of ignition depending on the system. It can indicate the ligand has reached its disassociation temperature and produced hypergolic byproducts, as in the case of urea and nitrate [50]. Depending on the phase that the reaction takes place in (solid, molten, gaseous) it can also indicate the transfer of reactants into the appropriate phase, as in the case of the gasification of hydrazine [51]. Regardless of the exact mechanism of a given system, the T_{ign} is often tuned through control of the precursor complex

13

and the ratio of oxidative to reductive components, though response to that tuning does depend on the mechanism.

This control of oxidative to reductive potential is conceptualized using theory based in propellant chemistry and jet propulsion [52]. Reported by Jain and Adiga, the process takes into account the individual oxidation number of elements in a reactant, whether it be in the ligand (the formal 'fuel') or counter ion (the formal 'oxidizer'). In this scheme elements are assigned oxidizing/reducing potential as follows [53].

Oxygen (-2)

Carbon (+4)

Hydrogen (+1)

Metal ion (+m)

Nitrogen (0)

Oxidizers are summed, and divided by reductants to yield the coefficient $\boldsymbol{\varphi}$ which describes the fuel-to-oxidizer ratio. At $\boldsymbol{\varphi} = 1$, the fuel and oxidizer are balanced and the reaction can proceed both at its highest exothermic release and without the addition of environmental oxygen. At $\boldsymbol{\varphi} > 1$, the precursor is fuel-lean and particles tend to be larger. At $\boldsymbol{\varphi} < 1$, the precursor is fuel-rich. This can lead to an excess of sooty reaction products from unreacted fuel, and/or in the case of strongly reducing fuels, zero valent metal products. This analysis is particularly useful when using multiple components as fuels have different reducing powers per mole. As well, from this type of analysis, it can be seen that the amount of fuel needed to chelate the metal (based in moles of fuel) and the amount of fuel needed to fully react

with nitrate (based in nature of fuel) are different, with 1:1 metal:ligand for homogenous chelation sometimes leading to large reducing excesses which are redox balanced via the addition of ammonium nitrate or nitric acid, NH_3NO_3 and HNO_3. If unbalanced, fuels source atmospheric oxygen for combustion, and mass transfer of oxygen into the reaction becomes a bottle neck for reaction time, pulling the system away from adiabatic conditions and reducing maximum reaction temperature.

Once solutions are made, there are different approaches to ignition. In the traditional SCS approach, solutions are heated on a hot plate or placed in a preheated furnace. The solution boils, continually thickening into what some call a 'gel' similar to a sol-gel reaction, until reaching ignition. Sometimes, precursors are dried into this 'gel' separately from their introduction into a hot furnace. Solutions can also be impregnated into solid supports which are either removed from combustion (alumina) or participate in it (cellulose), in techniques coined as Impregnated Layer Combustion Synthesis (ILCS) and Impregnated Active Layer Combustion Synthesis (IALCS) respectively[53]. The main separation between ILCS/IALCS is that, in IALCS reaction temperatures exceed the degradation temperature of the polymer. The substrate pyrolyzes, adding its own reaction heat to the local environment of the oxide-forming reaction, favoring high crystallinity and high temperature phases.

Once precursors are dried, impregnated, or otherwise put into a solid phase, heating is initiated either in Self-Sustaining High-Temperature Synthesis (SHS) or Volume Combustion Synthesis (VCS) regimes. In the SHS mode, there is limited preheating of the sample, before a hot metal wire, laser, or some other ignition source, is introduced into a spot. This creates a reaction, whose reaction heat allows the reaction to proceed across the whole sample in a

15

'reaction front'. In the VCS mode, the sample is heated uniformly across its volume up to the ignition temperature. This causes the whole sample to react at once. The SHS type reaction causes spatially resolved reaction zones (such as pre-reaction, reaction, and cooling zones) that make it possible to study the mechanism of reaction after quenching. The VCS mode is more straightforward and prevalent in the literature.

The primary methods of tuning combustion synthesis reactions (T_{ign}, phase, morph) are through the manipulation of **φ,** mixing of multiple fuels/metal salts, and the control of oxygen content in reaction atmosphere. The co-fuel effect has several contributors. The first is that fuels have different ignition temperatures, and a co-fuel can act as a lower temperature primer for a higher temperature combustion. The second is that mixed ligand complexes can be formed, with free (ligand exchanged) fuel molecules having differing critical temperatures. The third is that the separate burning of fuels like cellulose add their own heat to reaction, driving up the final adiabatic temperature, especially when present in excess as in IALCS [51].

Mukasyan and Dinka et al, after exploring these IALCS relations between cellulose and combustion precursors, produced a roll-to-roll process for the mass production of metal oxide nanoparticles[53]. In it, rolls of ash-less cellulose paper are sprayed with aqueous solutions of combustion precursor, dried, and ignited, with speeds of the rollers synched with the propagation speed of the reaction front. Produced hollow nanowires (in the shape of the cellulose fibers) were collected and ground.

Recently, Kim and Marks et al, used the solution combustion synthesis (in 2-methoxyethanol) to fabricate multilayer thin-film transistors (field effect) on a sheet. Subsequent simulations of the combustion reaction indicate that when precursors are deposited in thin enough layers in comparison to the substrate, that polymer substrates can soak the heat of

16

combustion (creating a cool zone that arrests the reaction front at the interface) without being driven into degradation temperatures [55]. This mirrors work by Mukasyan and Dinka in their experiments concerning the T_{ig} of ILCS synthesis of alumina supported catalysts, which showed decreases in T_{ig} at higher support/precursor ratios. For this reason, high- oxide forming, temperatures can be reached in the reaction without pyrolyzing the polymer substrate.

Cellulose

Chemically very similar to starch, cellulose is a natural biopolymer that has a long history of processing and use by humans. It is present in the basic industrial settings of agriculture and textile manufacture in the forms of raw cotton and rayon. As well, it is used in high technology applications like wound healing, lab-on-a-paper sensors, atomic level synthesis/mass transport control, and the production of templated nanomaterials [56]. This range of representation in the technical sphere has resulted in a wide and deep body of literature detailing cellulose processing conditions, properties, behaviors, and spectroscopic characteristics for researchers to draw from. As well, it means that updates to cellulose processing technologies will touch many different applications and economic sectors.

Containing five (5) oxygens per glucose monomer unit, cellulose has many of its physical and chemical properties defined by its hydrogen bonding and oxygen-rich character. It's well developed inter-chain hydrogen bonding network is responsible for its strong mechanical character, its noted resistance to dissolution, and its thermoset nature. Likewise, its oxygen rich nature creates an alcoholic surface character making cellulose a good adsorber of metal ions in solution. This surface character has been used to remediate heavy metal contaminated waters on environmental scales, but has less attention paid to adsorption on the consumer scale, where cellulose is invariably used as substrate for functional group grafting or inorganic loading.

In the past, this tendency to concentrate metal ions at its surface has been used to fabricate hollow metal oxide particles, including hollow wires and high fidelity 'fossils' of biological micro materials [57]. In that technique, cellulose containing materials are soaked in aqueous solutions of metal salts before firing at oxide forming temperatures, which caused cellulose to decompose. More recently, it has been explored explicitly as a cofuel in solution combustion precursor, and has shown to increase reaction temperatures through its highly exothermic pyrolysis.

Under heat treatment, cellulose remains unmelting until it burns at 350*C, with gaseous degradation beginning ~210*C. When pyrolyzed under a slow ramp rate (~10*C/min), cellulose first undergoes a limited hydrolysis to produce 'anhydrocellulose' [58]. The monomer units then begin to break down, releasing depolymerized cellulose (levoglucosane) as a reaction gas that can react with whole polymer chains in the bulk to produce carbonaceous char which remains after burning, the fraction of which can be increased by thermal pretreatment around 200*C. As a consequence of the high mass percent of oxygen in the polymer, this char is non-graphtizing. However, amorphous carbon produced through the hydrothermal carbonization of cellulose can be catalytically graphitized by nickel and nickel oxide in a solvation-reprecipitation mechanism [59].

The recalcitrance of cellulose to organic solvents means that most established techniques use one of two families of systems for cellulose processing. Solvated metal ions can intercalate into cellulose, where they interrupt the hydrogen bonding network via complex formation, allowing strong organics to solvate the polymer chains. Otherwise cellulose undergoes chemical alteration into one of its soluble derivatives (like cellulose acetate or carboxymethylcellulose), undergoes processing, and is then *regenerated* back into the original chemical structure via base

bath. Upon regeneration, cellulose is often amorphous and crystalline regions have their chains

stacked *anti* to each other (cellulose II phase), rather than parallel as in natural cellulose

(cellulose I phase).

Forcespinning

In addition to nano-effects present in the sub 100nm regime, nano and micro fibers are

desirable materials due to their high surface area, potential for high tensional strength, and

established compositing and processing techniques. Once produced, there are two main schools

of thought in how they are utilized. Fibers can be collected into a *tow*, or yarn, in which the

fibers are aligned axially and strongly associated. These tows can then be woven into a fabric or

wound into a spool. Similar to paper making, fibers can also be collected as a *nonwoven*, or felt,

in which the fibers are aligned randomly in a membrane hierarchy.

For applications affected by active surface area, like catalysis, adsorption, and

intercalation, the nonwoven morphology is the dominant form taken by fibers. This is especially

true as these applications often depend on inorganic compositing, and a free-standing nonwoven

is an excellent substrate for solving the problems ceramic particles have with contact, dispersion

and recovery in fluids.

A very popular technique for the lab-scale production of nanofiber nonwovens is

electrospinning. In that process, high voltages are applied, with a syringe of polymer solution

and a collector acting as electrodes [60]. The high potential difference causes ions in the polymer

solution to be repelled strongly from the surrounding needle-electrode, at the same time they are

attracted to the collector-electrode. This results in the formation of a 'Taylor Cone' of polymer

solution beaded at the tip of the needle, before the potential difference overcomes surface

tension, and jets of polymer solution arc to the collector. Solvent evaporates along the way, and a solid fiber results. This can produce small diameter fibers with tight size dispersion, but high voltages, ionic solutions, and especially the small mass of fiber produced inhibit the application of electrospinning to industrial production of technical fibers.

A technique with a greater potential for commercial application is Forcespinning. Forcespinning uses inertial forces to fling polymer jets through small diameter orifices (hypodermic needles) in a quickly rotating (1000-10,000 RPM) reservoir of polymer solution. These inertial forces 'shear thin' polymer jets into the micron-to-nm range diameter as the solution solvent evaporates to yield a solid fiber. This technique does not require electric fields, spins a wider array of polymers, and produces at least 3 orders of magnitude more fiber each minute compared with electrospinning [61].

Needle diameter and collector distance do play a lesser role, while the primary factors effecting fiber diameter are the RPM, viscoelasticity, and atmospheric conditions [62]. RPM is set by the experimenter on the machine. Defined by ratios like the Reynolds and Webber numbers, viscoelasticity is controlled by the wt% of the polymer solution, the molecular weight of the polymer, and solvent-solute interactions. These type solvent-solute interactions are adequately described by Hansen solubility parameters. Looking at these dispersion, polar, and hydrogen bonding parameters, we also see that polymer solutions will have different reactions to water, with atmospheric humidity acting either as solvent or antisolvent and the concentration of that water either favoring or disfavoring the evaporation of solvent from the polymer jet.

Fiber formation requires polymer solutions to be sufficiently viscoelastic, and for RPMs to pass a minimum threshold. Once both critical values are exceeded, a stream of polymer solution, of markedly smaller diameter than its aperture, exits the needle. It quickly elongates to

lengths longer than the dimensions of the chamber, and enters a holding position an equilibrium distance away from the spinneret where it continues to elongate and shear thin. Once it thins and loses enough solvent mass to become unstable in this equilibrium region, it moves farther from the spinneret where it is collected on foil wrapped posts.

During this time, the action of the polymer jet is partially describable by the action of spiraling liquid jets [65]. Here we see that, aside from the diameter, surface tension is vitally important to the system. The surface tensions of liquids drive them to make droplets in air, breaking up the stream into primary and satellite drops. Through the addition of small to moderate amounts of polymer, main drops can be connected through thin threads (which would have become satellite drops) in what is called the 'beads-on-a-string' morphology. Only when a sufficient wt% of polymer is added are jets able to form unbeaded fiber morphologies upon drying.

At the same time, the force of eddy currents in the chamber and the action of the spinneret introduce instabilities into the polymer jet/fiber which travel like vibrations up and down the length of the jet. These instabilities can be enough to break a polymer jet into droplets, especially when in conjunction with a high surface tension. So, to produce the fiber morphology from spiraling jets of polymer solution requires low surface tension, favorable atmosphere, RPM high enough to produce nanofiber but low enough not to destroy it, and viscosity high enough to maintain jet cohesion while still flowing enough to form a jet and thin.

In practice, atmosphere is made (perhaps imprecisely) 'wet' or 'dry' using a humidifier. Viable RPM's are between 2000-10,000 RPM. Polymer solutions are usually between 12-25 wt%, of as high a molecular weight as possible. Surface tension can be controlled with additives.

Coming together

Fine fibers (fibers of diameter 1um and below) have become increasingly important technologically. Even beyond textiles, they've found many applications, among them: sensors, energy storage, and water purification. Often, fibers serve as substrate for functionalization via chemical modification or inorganic loading.

Low temperature, room pressure methods of depositing ceramic materials on polymer fibers are dominated by solution methods, which can produce oxide coated and metallized fibers[65]. The drawbacks of these techniques are that they produce a liquid waste stream (in spent precursor solution), they require additional processing steps (like intensive washing), and they use toxic materials [66].

By using a simple chemical synthesis method which reduces waste streams, uses water as a solvent, proceeds at moderate temperatures, and *can coat large areas in ceramic material*, the explored chemistry can be readily upscaled. In consideration of this, the **solution combustion synthesis** is used to deposit ceramic shells on fibers. This technique is especially powerful in consideration of the Forcespinning method used to produce the nonwoven fiber mats used in this research.

As Forcespinning mass produces fine fibers, and the solution combustion synthesis can coat large areas at reduced cost, the conjunction of the two techniques can produce large areas/volumes of flexible and functionalized composite nonwovens. If composites have a high activity in applications, then materials will be strong contenders for materials in next generation devices.

CHAPTER III

INSTRUMENTATION

FE-SEM

Scanning Electron Microscopy (SEM) allows for the imaging of materials at scales smaller than is possible using light. In microscopy, the Rayleigh Criterion ($\theta = \frac{\lambda}{2NA}$) describes the resolving power of a given optical system. We see that the maximum resolving power is dependent on the wavelength used to image a system, with 404nm light being physically unable to image samples 100nm or below. However, as electrons have mass, their wavelength can be controlled by controlling their momentum. Thus, by accelerating electrons to a high enough speed, we can reduce their wavelength below 1nm. By making a beam of such electrons, we can direct it onto a sample, and detect resultant electron activity (backscattered and secondary electrons). In this way, SEM can be used to image features between 200um and 5nm.

It works in the following way: a very fine (micro) tungsten filament is heated to ~1850*K and subjected to kV extraction currents to produce a strong but diffuse beam of electrons via the Field Effect. This diffuse beam is accelerated by a potential difference with the stage and is focused through a series of objective and focusing magnetic lenses. These lenses are coils of wire which produce magnetic fields affecting the electrons, which are now in a beam. Between the objective and focusing lenses is an aperture set in a gold foil. This aperture collimates the beam, meaning that it excludes electrons with diagonal trajectories, bouncing them off the thin wall of

the pinholed foil. Smaller apertures produce a higher quality beam, but of lower intensity. The beam is focused onto the sample (making a conic shape), and rastered across the area of interest. The electrons are absorbed by the sample, and secondary electrons are released. These secondary electrons are collected by a charged-basket Everrett-Thornley type detector and an 'Inlens' detector set in the path of the beam, which can be used independently or in tandem. Penetration depth of electrons into the sample is controlled by acceleration voltage. It results in a trade off between image brightness and surface information, with lower acceleration voltages (kv=1) yielding dimmer images with more surface detail.

In this work, samples were imaged using a Carl-Zeiss Sigma VP FE-SEM with Gemini Optics. The beam was made under 9kv acceleration voltage (1kv from set voltage and 8kv from the 'super charger' in the path of the beam) and with a 7.5um aperture. For EDS analysis using an EDAX elemental analysis attachment, the aperture was widened to 30-120um and the acceleration voltage was increased to 13-15kv.

EDS

Energy Dispersive Spectroscopy (of X-Rays) is used to determine elemental composition of samples under an electron beam, and can be used to make a spatially resolved elemental map of samples, thanks to the rastering action of the electron beam in an SEM. When a sample absorbs an electron, that energy is transferred into the sample. There, that energy promotes inner shell electrons (K, L, M for innermost, second innermost, and third innermost shells). Those electrons can leave the sample to be absorbed as secondary electrons, become reabsorbed/reemitted/absorbed as sub-types of secondary electrons, or just become reabsorbed. When they are just reabsorbed, the excess energy is emitted as an X-ray. Because the energy of inner shell electrons is characteristic of elements, so is the emitted X-ray, allowing for elemental

analysis of samples. In this work, EDS was accomplished via an fin-cooled EDAX X-ray detector and TEAM analysis software.

XPS

Similar to EDS, X-ray Photoelectron Spectrophotometry (XPS) yields information on the energies of inner shell electrons of different elements. However, the resolution is much finer, allowing investigation of elemental information, but also bonding, and even geometry information through analysis of shielding/deshielding effects of local chemical environments. In this technique, X-rays are produced by bombarding a cooled metal foil with electrons to produce X-rays. These X-rays are run through slits to collimate, and are Bragg focused through an Al crystal onto the sample under vacuum. These high energy photons are absorbed by the sample, promoting inner shell (usually 1s or 2p) electrons. These free electrons are kicked off from the sample, captured by an acceleration voltage and subjected to a magnetic field. As moving charged particles in a magnetic field, their paths are deformed based on their kinetic energy in conformance with the right-hand rule. This results in their position of impact on the Si detector being tied directly with their kinetic energy as they exit the sample surface. By comparing this kinetic energy with the initial energy of the X-ray photons, rich information is yielded concerning the work function, ionization energy, bonding, local environment of elements, spin multiplicity, and other types of (sometimes exotic) information as subject to analysis.

Constant ejection of electrons can lead to sample surfaces developing positive charge, which affects the potential well that inner shell electrons must overcome to be ejected. This, in turn, effects the kinetic energy of ejected electrons, muddying the analysis of results with unknown modifications to barrier energy with time. To avoid this, samples are illuminated with an electron beam, or 'flood gun' to maintain charge neutrality in the sample.

25

In this work, a Thermo K-alpha XPS is used with analysis via Avantage software.

(ATR)-FTIR

Fourier Transform Infrared Spectroscopy is a type of vibrational spectroscopy used to determine the functional groups of molecules via the energy of their vibrations (which correspond to frequencies of absorbed photons), with the number and type of vibrations being determined by a given molecule's symmetry. In this technique, a wide spectrum beam of radiation is transmitted through a sample while undergoing frequency modulation. The detected signal is transformed into a Fourier series composed of terms describing each frequency contribution. Reductions in term coefficients with respect to a reference indicate absorption by the sample at that frequency.

Traditionally, powdered samples are suspended in pellets of IR transparent KBr which are set in the path of the beam. Free standing membranes can also be set neat in the path of the beam, if they are sufficiently thin so as to transmit some light. As well, a newer technique called Attenuated Total Reflection FITR (ATR-FTIR) uses total internal reflection to analyze the surface of solid materials with minimal sample handling. In this technique, the sample is flush with a crystal which has light beam shown through it. This light reflects off the sample into the detector, with an evanescent wave (which slightly penetrates into the sample) accounting for the portion which is absorbed by the sample. In this work, a 'Vertex 10' ATR-FTIR is used

GFAA

Graphite Furnace Atomic Absorption spectrophotometry (GFAA) is an absorption based technique which is used to determine absorption of specific metals at solution concentrations as low as 0-10 ppb. In this technique, samples are processed into acidified aqueous solutions. Each

of these solutions, a blank, and 3 calibration standards are loaded into an automated sample wheel. From this wheel, solutions are fed via capillary tube into a hollow graphite tube. This tube is heated via resistance heating, first to evaporate the water of the solution, and then to high temperatures in order to vaporize sample ions into a plasma. This plasma cools into a solid aerosol in the path of a beam. This beam is produced by sputtering the same element under analysis. Because of this, the wavelength of the produced light is of very narrow wavelength distribution and of the exact wavelength of analyte absorption. This is what allows analysis of concentrations of such low concentration. The resultant beam is detected, and the solid aerosol is evacuated via vent.

In this work, acidified aqueous samples are analyzed via Perkin Elmer AA900 in graphite furnace mode, before and after batch type adsorption. Differences in concentration are translated into adsorption capacity in mg/g.

CHAPTER IV

EXPERIMENTAL PROCEDURE

Acetone and Dimethylacetamide are mixed to make a 2:1 v/v solvent. This mixed solvent is used to dissolve Cellullose Acetate (CA) (30,000 MW) and Polyvinylpyrrolidone (PVP) (1,000,000 MW) making 12-21 wt% solutions at 1, 2, and 3 wt% PVP. Solutions are briefly vortexed to roughly combine components and left to stir for 48 hours in a scintillation vial using a tightly fitting stirbar.

When mirage fingers are no longer visible (indicating homogeneous density), polymer solutions are Forcespun. 2ml of solution are loaded into a 24-gauge needled, two-headed type metal spinneret and spun at 1000RPM increments between 3000-9000 RPM using an L-1000 Cyclone. Approximately 13 cm from the needles, fibers are caught on foil wrapped posts. From the posts, fibers are formed into loose nonwoven mats by roll-collecting with a foil wrapped piece of cardboard or 3d-printed roller drum tool.

The best resultant CA nonwovens are soaked in 3wt% KOH/EtOH$_{(95\%)}$ solutions overnight to regenerate cellulose acetate into cellulose, that is, the acetyl functional groups of cellulose acetate are replaced by the hydroxyl functional groups. Regenerated membranes soak in successive baths of deionized water until registering the pH of still water (~6) to pH paper. They are then dried at 100*C.

Solution combustion precursors are prepared by mixing iron nitrate nonahydrate with different fuel mixtures (acetylacetone, urea, acetylacetone/urea, urea/ammonium chloride) at different ratios to give solutions which were redox balanced, fuel rich, or fuel lean, and adding water until complete dissolution.

Cellulose membranes are briefly dipped in precursor solutions. Using a kimwipe, samples are either patted to dampness, or well pressed until no more liquid is removed. Precursor loaded membranes are then placed on a glass bowl in an oven preheated to 190-220*C for around 1min. Upon removal, composite membranes are washed with water, and dried at 100*C.

Lead adsorption properties are tested by batch type adsorption of lead acetate at concentrations between 0-500 ppb, using 2-4mg of adsorbent and solution:adsorbent ratio of 3000. Lead solutions are made by dissolving lead acetate in deionized water to make a 500ppb solution which is diluted to all other concentrations. Triplicates of each composite sample soak for 24 hours with limited agitation to establish equilibrium. Solutions are filtered through 0.4 micrometer PTFE pore syringe filters, acidified with nitric acid, and analyzed via Graphite Furnace Atomic Adsorption spectrophotometry (GFAA). Throughout adsorption testing, glass is avoided in favor of polypropylene to prevent incidental adsorption of metal ions.

FTIR, SEM, and XPS analysis are conducted on every sample (CA, cellulose, precursor mat, composite mat, post adsorption mat).

CHAPTER V

RESULTS AND DISCUSSION

Fiber Nonwovens and Pores

Figure 1 shows the resultant quality of fibers at corresponding PVP wt%, total polymer wt%, and RPM. At the lowest overall percent weight of 12wt% PVP and Cellulose Acetate, no fibers were formed under any conditions. At 15wt%, fibers were formed best at low RPMs and were broken apart at higher RPMs via mechanisms discussed in the literature review. As the percent weight of the solutions increased, the RPM at optimal fiber formation increased up to 6000 RPM.

The best samples of each run are separated for SEM analysis of fiber diameter, and select results are presented in Figure 2. Samples most suitable for mat formation were voluminous, free from flecks, visually fine, virtually without bead-on-a-string morphologies under SEM, and with fiber diameters around 1 micrometer. FTIR analysis of as-spun cellulose acetate and regenerated cellulose fibers are shown in Figure 4 depict a total removal of the absorptions @ (1737/cm) and (1217/cm) characteristic of the carbonyl functional group. At the same time, we see a growth in the 3000-3500/cm region characteristic of hydroxyl stretches. These indicate the acetyl groups of the triacetylcellulose have been fully converted to the (-OH) groups of cellulose.

FTIR vibrations characteristic of PVP at (1650, 1370, and 570) were present in the FTIR. As well, XPS measurements show nitrogen signals present in regenerated cellulose samples. This

N 1s signal is deconvoluted into substituent peaks at 398.98, 399.28, and 401.18 eV. While there are three nitrogen species in PVP, these do not correspond to their values present in the literature [66]. While PVP is soluble in both water and ethanol and should be stripped, PVP reactions with strong bases can lead to dangling pendant groups and chemical reaction. The 2% PVP samples were used for all further characterizations and steps.

During cellulose regeneration, bulky acetyl groups are replaced with much less steric hydroxy groups. Dealing with just the cellulose acetate polymer, this would entail reduction in both weight and volume of the solid polymer phase. It is this system of mass transport which is responsible for porosity of the regenerated cellulose fibers.

Pore size can be difficult to determine via SEM, but surface pores appear to be around 60nm and below. Images of fiber cross sections Figure 10 show the pore structure extends through to the center of fibers. In addition to the alcoholic surface character of the cellulose, it is this porous structure, and the accompanying high surface area that are responsible for its adsorption activity.

Composites

If substrate temperatures reach the cellulose pyrolysis temperature of 350*C, the cellulose fibers combust, leaving behind vivid red samples of nanoparticles aggregated into hollow wires as shown in Figure 5. XPS analysis of O 1s signals confirm these wires as Iron Oxide from the characteristic signal below 530 ev. As mentioned, this result, where cellulose is used as a pyrolyzed substrate, has been well established by groups in different contexts.

By reducing the loading of combustion precursor, the total reaction temperature can be reduced below the level of cellulose pyrolysis. This is accomplished in our work by a vigorous

pinch between kimwipes. This leaves behind only the aqueous solution which is well bonded and does not de-wet from the surface of nonwoven fibers onto dry kimwipes. As a result, thermal treatment results in an unburnt cellulose-composite. Under SEM Figure 6, samples appear very similar to neat cellulose fibers Figure 3, but with the suggestion of partial pore filling on the fiber surface, and the creation of ridges where two fibers merged into one during spinning or regeneration Figure 10. EDS investigation shows iron and nitrogen present homogeneously throughout fibers.

XPS analysis of composite O 1s signals indicate that there is no metal oxide present, due to the absence of characteristic oxide peaks <530 eV. Deconvolution of N 1s Figure 12 signals show additional peaks at 397.68 eV, 399.58 eV, and 400.18 eV which are indicative of metal nitride, and nitrogen in two different NO+ oxidized species respectively [67]. As well, Fe 2p signals show a suppression of satellite peaks between 710-720 eV which indicate the formation of low spin metal complexes, giving evidence for M-N bonding. Compared with pyrolyzed samples, composites show a red shift in the Fe P 3/2 peak and blue shift in the Fe P ½ peak, showing an increase in Fe 2p spin-orbit splitting by 1.2 eV.

In total, XPS analysis of O 1s, N 1s, and Fe 2p signals indicate that the inorganic portion of composites consists of an Fe(III) nitride material. SEM and EDS analysis show that this inorganic portion is of high fidelity with the cellulose fibers, but not in a distinct core-shell structure. These results are in agreement with reports of cellulose's ability to act as a high fidelity template for metal ions, and of urea to act as nitrogen precursor to metal nitride materials.

Multiple soaking-drying-firing cycles are performed on samples to induce growth of inorganic portions. Morphologically, these portions are present as webs bonding fibers together,

as can be seen in Figure 7. EDS analysis confirms that these portions do not contain carbon, but do contain Fe, N, and O.

SEM images of crude Zinc samples are included in Figure 9. In it we see well developed inorganic phases and uncontrolled shell formation.

Adsorption

3 sample types were chosen for initial, unagitated batch type adsorption testing of Pb^{2+} : Regenerated Cellulose, Single Process Fuel Rich Iron/Acetylacetone/Urea(1:1:3), and Single Process Zinc/Urea/NH$_4$Cl. Triplicate samples of cellulose and iron-composite were used, and a single sample of zinc-composite. Results are presented in table 1

Sample	InitialConcentration(ppb)	FinalConcentration(ppb)	ΔConcentration(ppb)	Loading(mg/g)
Zinc composite	120.00	89.40	30.6	22.9
Iron composite	98.90	40.27	58.63	175.89
Iron composite	98.90	14.38	84.52	253.56
Iron composite	98.90	24.31	74.59	223.77
Regenerated Cellulose	98.90	3.26	95.64	286.92
Regenerated Cellulose	98.90	1.68	97.22	291.66
Regenerated Cellulose	98.90	1.26	97.64	292.92

From this table, we see that samples show average loading capacities of 217.74 mg/g of Pb^{2+} onto iron composite samples and 290.59 mg/g for regenerated cellulose. These values compare favorably with literature. Zinc samples were not further investigated.

Plotting adsorption data taken at different initial concentrations, and the resultant mg/g loading capacity of the adsorbents, (mg/g loading _vs_ initial concentration), we see simple, Henry type adsorption isotherms Figure 13 This means that there is a simple linear relationship between initial concentration and adsorption capacity and is consistent with a system in a dilute regime, as ours is. Percentage adsorption and adsorption capacity data is presented in Figure 14 At the lowest concentration regime of <10 ppb, Adsorption capacities for regenerated cellulose and cellulose-composites were 26.05 and 15.72 mg/g respectively. At the highest concentration near 500 ppb, capacities for cellulose and cellulose composites were 1351 and 1210 mg/g respectively. This is very high adsorption activity and bears further investigation.

Comparing cellulose and composite samples, we see a 40% reduction in adsorption capacity in the most dilute regime. As the initial concentration of lead solutions increase, this difference in capacity decreases until reaching 10% in the highest concentration samples. There are two methods by which the iron material may cause this reduction. The first, is through pore filling. This reduces the surface groups available for adsorption. The second is through differential lead affinities between cellulose and the ceramic, resulting from differing chemical compositions. The total difference between samples is likely to be as a combination of both.

To further investigate the nature of adsorption, data were plotted using linearized forms of the Langmuir, Freundlich, and Dubinin–Radushkevich equations, similar to other investigators (22).

Plots of equilibrium concentration (Ce) divided by adsorption capacity (qe) vs equilibrium concentration {Langmuir}, ln(qe) vs ln(Ce) {Freundlich}, and ln(qe) vs (RTln(1+1/Ce))^2 {D-R} are included in Figures 15-17

From these plots of terms from linear expressions, we see that Langmuir modeling gives no relation, Frendlich modeling gives a poorly fitted linear relation for cellulose but a passable one for composite samples , and D-R modeling gives a well-fit linear relation for both. To show this linear D-R relation, the lowest concentration samples (below 10 ppb) had to be excluded as the empirical D-R relationship is not applicable to very dilute regimes (i.e. under 10ppb). The good fit using the linearized Dubinin-Radushkevich equation suggests that nanopores may be contribute to Pb-ion adsorption beyond increases surface area, though the original formulation of the D-R expression for gases make this comparison possibly deceptive.

CHAPTER VI

CONCLUSIONS

The objective of producing lead adsorption membranes with a reduced time/resource cost and high adsorption capacity was successful. Cellulose fiber nonwovens brought water leaded from 25-times the coming Federal Action Limit of 10 ppb (248.9 ppb) to drinkability (10 ppb and below). This is represented by adsorption capacities in excess of 1000 mg/g , meaning that samples contain more adsorbed lead by weight than cellulose. This reduction in lead ion concentration was accomplished at an adsorbent:solution ratio of 1:3000, room temperature, and the pH of still water. As well, nonwovens were produced using methods which are up-scalable and show favorable resource consumption when compared with commercial activated carbon materials in literature.

The objective of controlling parameters to induce core/shell morphologies in cellulose/ceramic composite fiber membranes was unsuccessful. Though iron nitride was repeatedly formed on fibers, and some samples showed ceramic shells, shell could not be controllably induced. Instead, most samples showed morphologies which were not appreciably changed, but with Fe and N distributed throughout. When separate phases could be controllably induced, they did not form shells.

Taking into account the high adsorption activity, common material, ceramic deposition, and uncontrolled morphology; the project is an overall partial success. Moving forward, more in-depth analysis of adsorption behavior is required, with larger range of adsorption data (into

36

the ppm) analyzed with many different isotherm expressions. As ceramic functionalization results in reductions of overall capacity, composite materials should be tested for superior

selectivity to target adsorbents, rather than raw capacity. Morphology control should be attempted with better control of precursor loading, and the variation of fuel used. Ceramic identity should be altered through the variance of the oxidative-reductive (ie, the addition of nitric acid) as well as the variation of fuel.

Progress on objective 2 (energy storage) can begin by carbonizing composite samples under nitrogen flow for testing. Cellulose is non-graphitizing, but ceramic particles have been shown to dissolve amorphous carbon and reprecipitate it as graphite. Thermal treatment of composite mats, with and without thermal pretreatment should be explored, followed by the incorporation into coin cells of suitable samples. Data produced in this experiment will give further insight into the nature and ability of the composite fibers, necessary for advancement into objective 3.

REFERENCES

1. Needleman, Herbert. "Lead poisoning." *Annu. Rev. Med.* 55 (2004): 209-222.

2. Reuben, Aaron, Jonathan D. Schaefer, Terrie E. Moffitt, Jonathan Broadbent, Honalee

3. Harrington, Renate M. Houts, Sandhya Ramrakha, Richie Poulton, and Avshalom Caspi. "Association of childhood lead exposure with adult personality traits and lifelong mental health." *JAMA psychiatry* 76, no. 4 (2019): 418-425

4. Nevin, R. (2000). How lead exposure relates to temporal changes in IQ, violent crime, and unwed pregnancy. Environmental research, 83(1), 1-22.

5. Pocock, S. J., Shaper, A. G., Walker, M., Wale, C. J., Clayton, B., Delves, T., ... & Powell, P. (1983). Effects of tap water lead, water hardness, alcohol, and cigarettes on blood lead concentrations. Journal of Epidemiology & Community Health, 37(1), 1-7.\

6. "Lead and Copper Rule", 40 C.F.R § 141 (2019)

7. Brown, M. J., & Margolis, S. (2012). Lead in drinking water and human blood lead levels in the United States.

8. Source: Agency for Toxic Substances and Disease Registry

9. U.S. Environmental Protection Agency (2016) "Lead and Copper Rule Revisions" White paper describing rational reasoning, and projected outcomes for proposed revisions to the federal Lead and Copper Rule"

10. https://www.epa.gov/sites/production/files/2016-10/documents/508_lcr_revisions_white_paper_final_10.26.16.pdf (accessed: 12/2019)

11. Raymond, J., Wheeler, W., & Brown, M. J. (2014). Lead screening and prevalence of blood lead levels in children aged 1–2 years—Child blood lead surveillance system, United States, 2002–2010 and national health and nutrition examination survey, United States, 1999–2010. Morbidity and mortality weekly report, 63(2), 36-42.

12. Hanna-Attisha, M., LaChance, J., Sadler, R. C., & Champney Schnepp, A. (2016). Elevated blood lead levels in children associated with the Flint drinking water crisis: a spatial analysis of risk and public health response. American journal of public health, 106(2), 283-290.

13. Maher, John A. "Lead poisoning more likely for Pennsylvania children than in Flint, Michigan." Youtube video, 2:49. (2016). https://youtu.be/Ug0bhvtvgzU

14. Frostenson, Sarah "18 cities in Pennsylvania reported higher levels of lead exposure than Flint" Vox (2016). https://www.vox.com/2016/2/3/10904120/lead-exposure-flint-pennsylvania

15. Dep. of Health, Pennsylvania, "2014 Childhood Lead Surveillance Annual Report" PA: United States (2014)

16. Edwards, M., Triantafyllidou, S., & Best, D. (2009). Elevated blood lead in young children due to lead-contaminated drinking water: Washington, DC, 2001− 2004. Environmental science & technology, 43(5), 1618-1623.

17. Li, T., Dai, Y. H., Xie, X. H., Tan, Z. W., Zhang, S. M., & Zhu, Z. H. (2014). Surveillance of childhood blood lead levels in 11 cities of China. World Journal of Pediatrics, 10(1), 29-37.

18. Zejda, J. E., Grabecki, J., Krol, B., Panasiuk, Z., Jedrzejczak, A., & Jarkowski, M. (1997). Blood lead levels in urban children of Katowice Voivodship, Poland: results of the population-based biomonitoring and surveillance program. Central European journal of public health, 5(2), 60-64

19. Centers for Disease Control and Prevention (CDC. "Blood lead levels in residents of homes with elevated lead in tap water--District of Columbia, 2004." *MMWR. Morbidity and mortality weekly report* 53.12 (2004): 268.

20. Carol D. Leonning, (2010) 'CDC misled District residents about lead levels in water, House probe finds' Washington Post, 05/20, https://www.washingtonpost.com/wp-dyn/content/article/2010/05/19/AR2010051902599.html?wprss=rss_print&sid=ST2009021100308

21. Ayawei, Nimibofa, Augustus Newton Ebelegi, and Donbebe Wankasi. "Modelling and interpretation of adsorption isotherms." Journal of Chemistry 2017 (2017).

22. Liu, Junsheng, and Xin Wang. "Novel silica-based hybrid adsorbents: lead (II) adsorption isotherms." The Scientific World Journal 2013 (2013).

23. Gonte, Renuka R., K. Balasubramanian, and Jyothi D. Mumbrekar. "Porous and cross-linked cellulose beads for toxic metal ion removal: Hg (II) ions." Journal of Polymers 2013 (2013).

24. Yang, Rui, et al. "Thiol-modified cellulose nanofibrous composite membranes for chromium (VI) and lead (II) adsorption." *Polymer* 55.5 (2014): 1167-1176.

25. Ma, Hongyang, Benjamin S. Hsiao, and Benjamin Chu. "Electrospun nanofibrous membrane for heavy metal ion adsorption." *Current Organic Chemistry* 17.13 (2013): 1361-1370.

26. Wang, Ran, et al. "Nanofibrous microfiltration membranes capable of removing bacteria, viruses and heavy metal ions." *Journal of Membrane Science* 446 (2013): 376-382.

27. Wu, Chunlin, et al. "Polydopamine-mediated surface functionalization of electrospun nanofibrous membranes: preparation, characterization and their adsorption properties towards heavy metal ions." *Applied Surface Science* 346 (2015): 207-215.

28. Mishra, P. C., & Patel, R. K. (2009). Removal of lead and zinc ions from water by low cost adsorbents. Journal of Hazardous Materials, 168(1), 319-325.

29. Yu, B., Zhang, Y., Shukla, A., Shukla, S. S., & Dorris, K. L. (2001). The removal of heavy metals from aqueous solutions by sawdust adsorption—removal of lead and comparison of its adsorption with copper. Journal of hazardous materials, 84(1), 83-94.

30. Feng, Q., Lin, Q., Gong, F., Sugita, S., & Shoya, M. (2004). Adsorption of lead and mercury by rice husk ash. Journal of colloid and interface science, 278(1), 1-8.

31. Zulkali, M. M. D., Ahmad, A. L., & Norulakmal, N. H. (2006). Oryza sativa L. husk as heavy metal adsorbent: optimization with lead as model solution. Bioresource technology, 97(1), 21-25.

32. Abdulrasaq, O. O., & Basiru, O. G. (2010). Removal of copper (II), iron (III) and lead (II) ions from mono-component simulated waste effluent by adsorption on coconut husk. African Journal of Environmental Science and Technology, 4(6).

33. Khalid, N., Ahmad, S., Kiani, S. N., & Ahmed, J. (1998). Removal of lead from aqueous solutions using rice husk. Separation science and technology, 33(15), 2349-2362.

34. Tokimoto, T., Kawasaki, N., Nakamura, T., Akutagawa, J., & Tanada, S. (2005). Removal of lead ions in drinking water by coffee grounds as vegetable biomass. Journal of Colloid and interface Science, 281(1), 56-61.

35. Mehta, S. K., & Gaur, J. P. (2005). Use of algae for removing heavy metal ions from wastewater: progress and prospects. Critical reviews in biotechnology, 25(3), 113-152.

36. Bhattacharyya, K. G., & Gupta, S. S. (2008). Adsorption of a few heavy metals on natural and modified kaolinite and montmorillonite: a review. Advances in colloid and interface science, 140(2), 114-131.

37. Hua, M., Zhang, S., Pan, B., Zhang, W., Lv, L., & Zhang, Q. (2012). Heavy metal removal from water/wastewater by nanosized metal oxides: a review. Journal of hazardous materials, 211, 317-331.

38. Liu, C., & Huang, P. M. (2003). Kinetics of lead adsorption by iron oxides formed under the influence of citrate. Geochimica et Cosmochimica Acta, 67(5), 1045-1054.

39. Kooner, Z. S. (1993). Comparative study of adsorption behavior of copper, lead, and zinc onto goethite in aqueous systems. Environmental Geology, 21(4), 242-250.

40. Nelson, Y. M., Lion, L. W., Shuler, M. L., & Ghiorse, W. C. (2002). Effect of oxide formation mechanisms on lead adsorption by biogenic manganese (hydr) oxides, iron (hydr) oxides, and their mixtures. Environmental science & technology, 36(3), 421-425.

41. Kumar, K. Y., Muralidhara, H. B., Nayaka, Y. A., Balasubramanyam, J., & Hanumanthappa, H. (2013). Low-cost synthesis of metal oxide nanoparticles and their application in adsorption of commercial dye and heavy metal ion in aqueous solution. Powder technology, 246, 125-136.

42. Goel, J., Kadirvelu, K., Rajagopal, C., & Garg, V. K. (2005). Removal of lead (II) by adsorption using treated granular activated carbon: batch and column studies. Journal of hazardous materials, 125(1-3), 211-220.

43. Largitte, L., & Pasquier, R. (2016). A review of the kinetics adsorption models and their application to the adsorption of lead by an activated carbon. Chemical Engineering Research and Design, 109, 495-504.

44. Zhang, K., Cheung, W. H., & Valix, M. (2005). Roles of physical and chemical properties of activated carbon in the adsorption of lead ions. Chemosphere, 60(8), 1129-1140.

45. Merzhanov, Alexander G. "The chemistry of self-propagating high-temperature synthesis." *Journal of Materials Chemistry* 14.12 (2004): 1779-1786.

46. Martirosyan, Karen S., and Dan Luss. "Carbon combustion synthesis of ferrites: synthesis and characterization." *Industrial & engineering chemistry research* 46.5 (2007): 1492-1499.

47. Varma, Arvind, et al. "Solution combustion synthesis of nanoscale materials." *Chemical reviews* 116.23 (2016): 14493-14586.

48. Kingsley, J. J., and K. C. Patil. "A novel combustion process for the synthesis of fine particle α-alumina and related oxide materials." *Materials Letters* 6.11-12 (1988): 427-432.

49. Wen, Wei, and Jin-Ming Wu. "Nanomaterials via solution combustion synthesis: a step nearer to controllability." *RSC Advances* 4.101 (2014): 58090-58100.

50. Tokmakov, Igor V., Saman Alavi, and Donald L. Thompson. "Urea and urea nitrate decomposition pathways: A quantum chemistry study." *The Journal of Physical Chemistry A* 110.8 (2006): 2759-2770.

51. Deshpande, Kishori, Alexander Mukasyan, and Arvind Varma. "Direct synthesis of iron oxide nanopowders by the combustion approach: reaction mechanism and properties." *Chemistry of materials* 16.24 (2004): 4896-4904.

52. Jain, S. R., K. C. Adiga, and VR Pai Verneker. "A new approach to thermochemical calculations of condensed fuel-oxidizer mixtures." *Combustion and flame* 40 (1981): 71-79.

53. Mukasyan, A. S., and P. Dinka. "Novel approaches to solution-combustion synthesis of nanomaterials." *International Journal of Self-Propagating High-Temperature Synthesis* 16.1 (2007): 23-35.

54. Kim, Myung-Gil, et al. "Low-temperature fabrication of high-performance metal oxide thin-film electronics via combustion processing." *Nature materials* 10.5 (2011): 382-388.

55. Sanchez-Rodriguez, Daniel, et al. "Thermal analysis for low temperature synthesis of oxide thin films from chemical solutions." *The Journal of Physical Chemistry C* 117.39 (2013): 20133-20138.

56. Moon, Robert J., et al. "Cellulose nanomaterials review: structure, properties and nanocomposites." *Chemical Society Reviews* 40.7 (2011): 3941-3994.

57. Huang, Jianguo, and Toyoki Kunitake. "Nano-precision replication of natural cellulosic substances by metal oxides." *Journal of the American Chemical Society* 125.39 (2003): 11834-11835.

58. Shen, D. K., and Sai Gu. "The mechanism for thermal decomposition of cellulose and its main products." *Bioresource technology* 100.24 (2009): 6496-6504.

59. Foresti, María Laura, Analía Vázquez, and Bruno Boury. "Applications of bacterial cellulose as precursor of carbon and composites with metal oxide, metal sulfide and metal nanoparticles: A review of recent advances." *Carbohydrate polymers* 157 (2017): 447-467.

60. Sarkar, Kamal, et al. "Electrospinning to forcespinning™." *Materials today* 13.11 (2010): 12-14.

61. Weng, Baicheng, et al. "Fibrous cellulose membrane mass produced via forcespinning® for lithium-ion battery separators." *Cellulose* 22.2 (2015): 1311-1320.

62. Padron, Simon, et al. "Experimental study of nanofiber production through forcespinning." *Journal of applied physics* 113.2 (2013): 024318.

63. Wong, D. C. Y., et al. "Break-up dynamics and drop size distributions created from spiralling liquid jets." *International journal of multiphase flow* 30.5 (2004): 499-520.

64. Părău, E. I., et al. "Nonlinear travelling waves on a spiralling liquid jet." *Wave Motion* 43.7 (2006): 599-618.

65. Drew, Christopher, et al. "Metal oxide-coated polymer nanofibers." *Nano Letters* 3.2 (2003): 143-147.

66. Wang, Lili, et al. "Bio-Multifunctional Smart Wearable Sensors for Medical Devices." *Advanced Intelligent Systems* 1.5 (2019): 1900040.

67. Wan, Ling-Shu, Zhi-Kang Xu, and Zhen-Gang Wang. "Leaching of PVP from polyacrylonitrile/PVP blending membranes: a comparative study of asymmetric and dense membranes." *Journal of Polymer Science Part B: Polymer Physics* 44, no. 10 (2006): 1490-1498.

68. Torres, Jessica, C. C. Perry, Stephen J. Bransfield, and D. Howard Fairbrother. "Low-temperature oxidation of nitrided iron surfaces." *The Journal of Physical Chemistry B* 107, no. 23 (2003): 5558-5567.
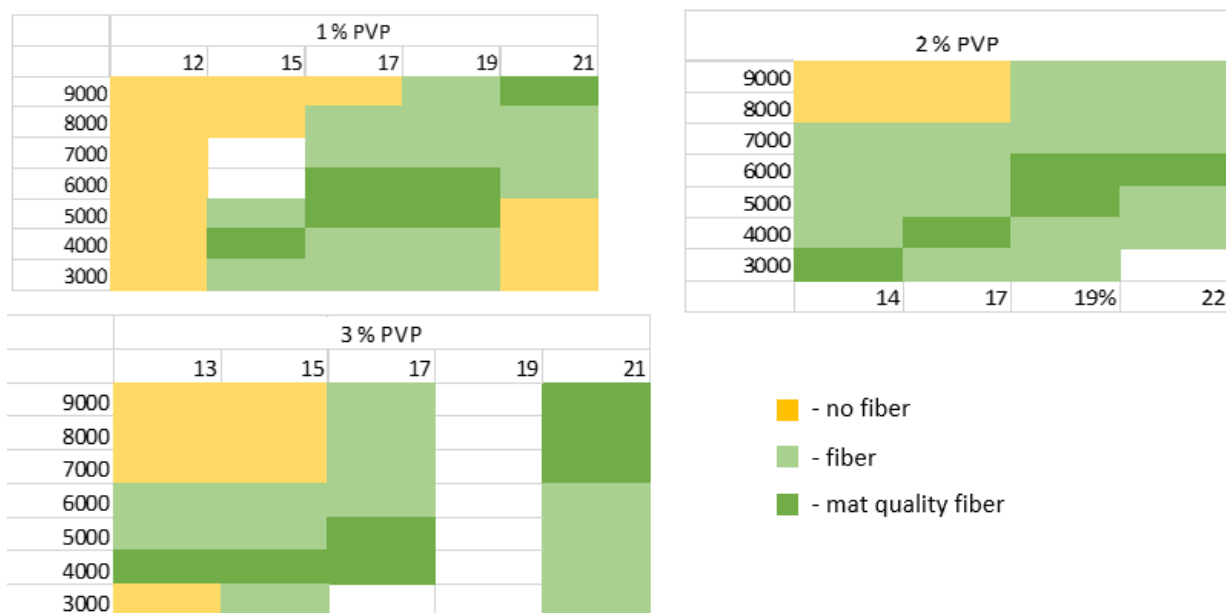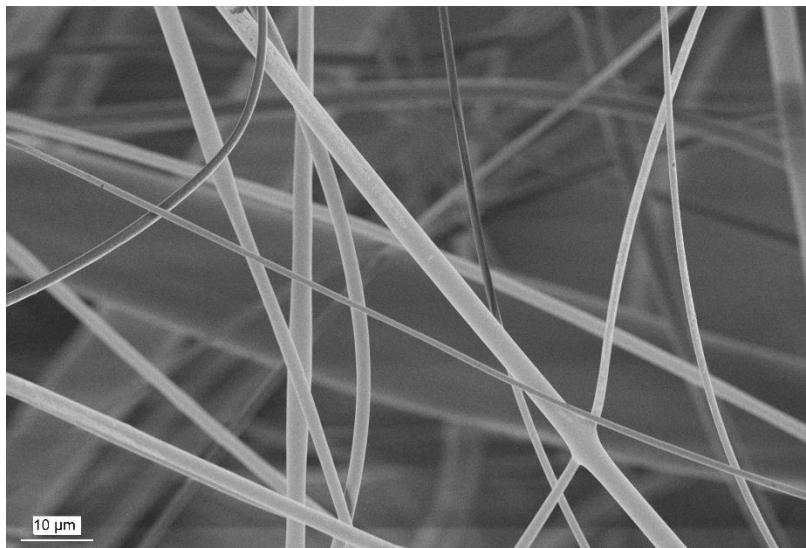
APPENDIX A

1 % PVP

	12	15	17	19	21
9000					
8000					
7000					
6000					
5000					
4000					
3000					

2 % PVP

	14	17	19%	22
9000				
8000				
7000				
6000				
5000				
4000				
3000				

3 % PVP

	13	15	17	19	21
9000					
8000					
7000					
6000					
5000					
4000					
3000					

- no fiber
- fiber
- mat quality fiber

Fig 1)

Fig 2) As-spun Cellulose Acetate fibers
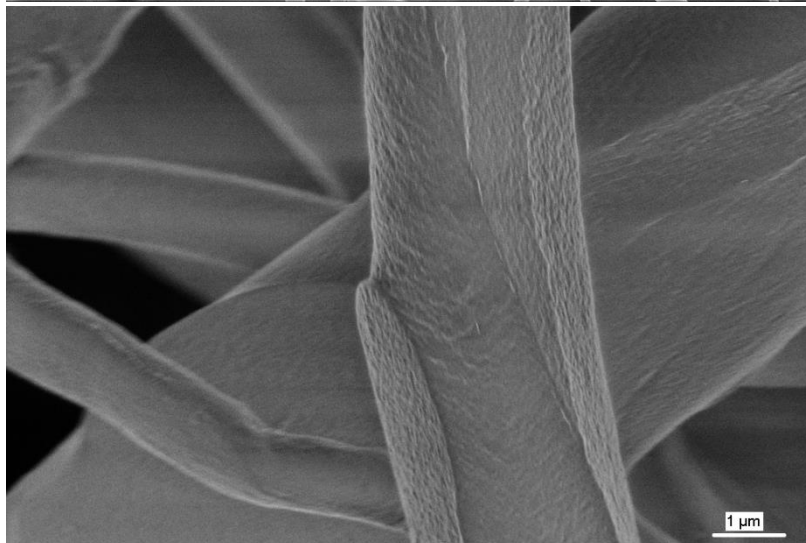
Fig 3) Regenerated Cellulose Fiber
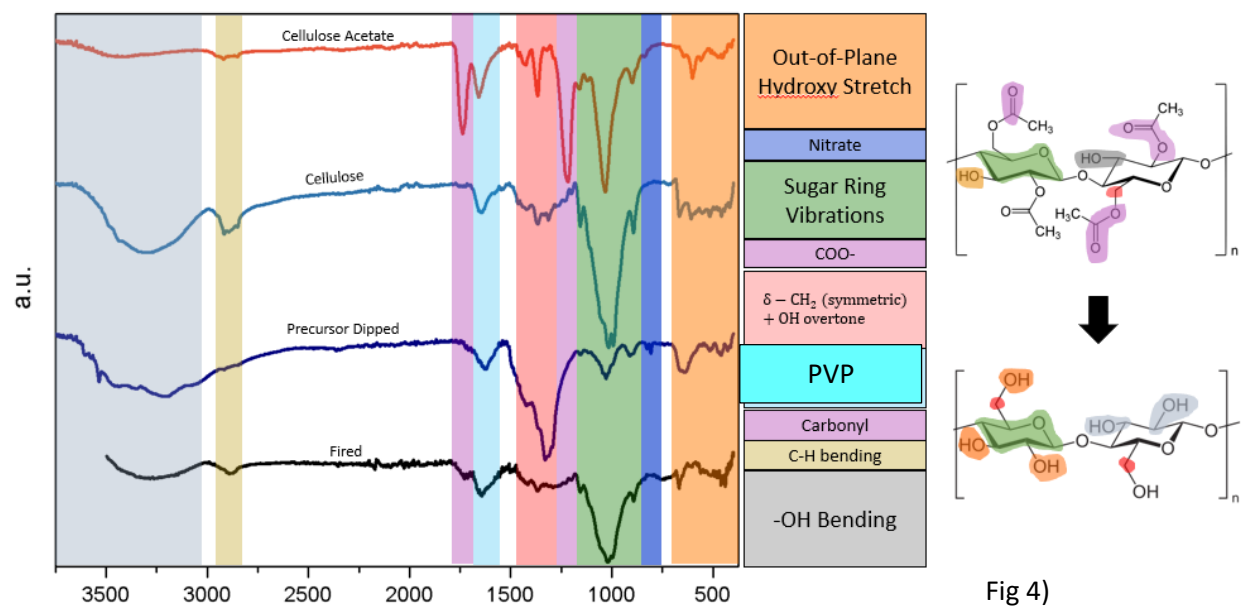
Fig 4)

FTIR Analysis of CA, Regenerated, Precursor Dipped, and Fired samples
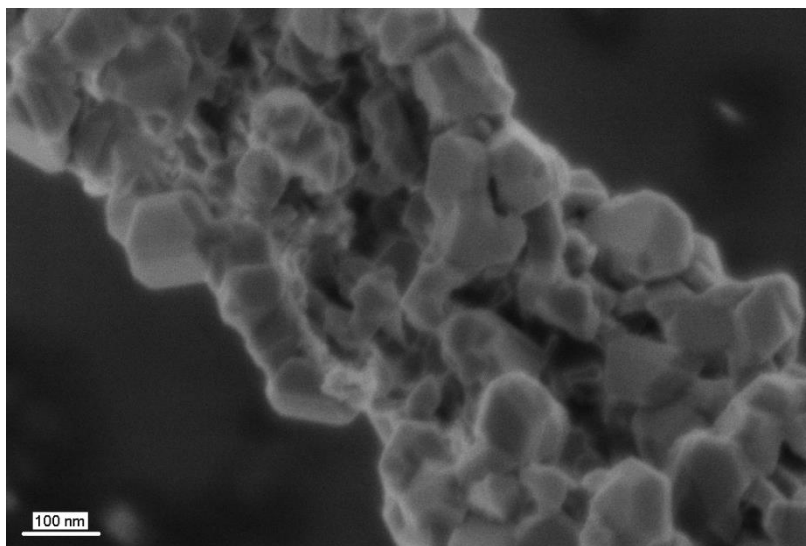
Fig 5) Iron Oxide nanoparticles aggregated in the form of a precursor soaked fiber which has pyrolyzed
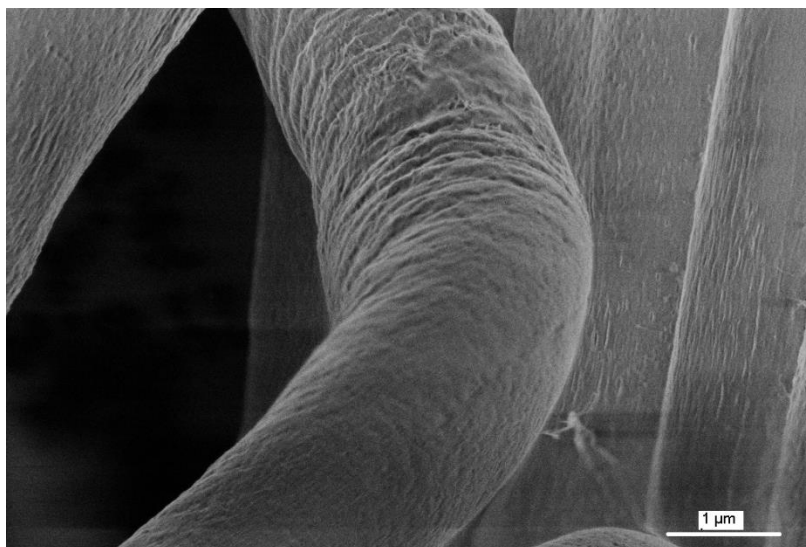
Fig 6) Cellulose-Iron ceramic composite. Cellulose remains unpyrolyzed
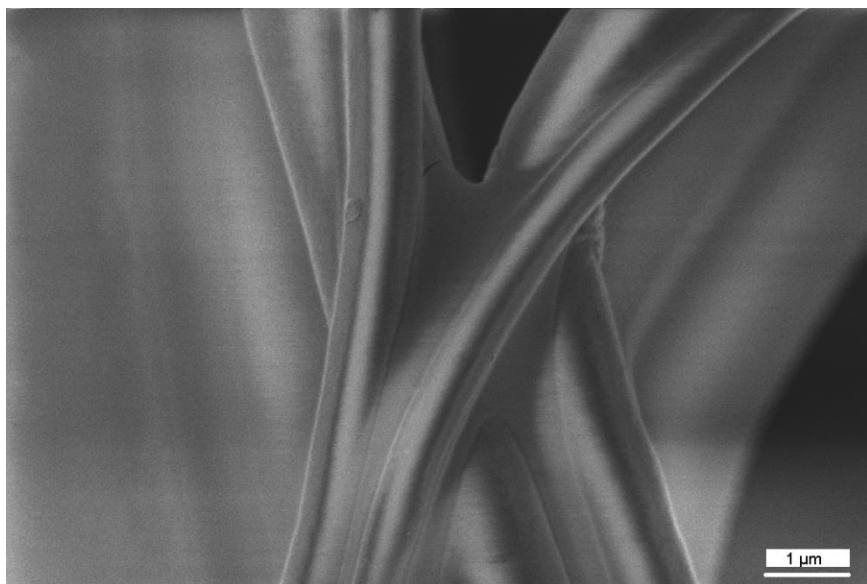
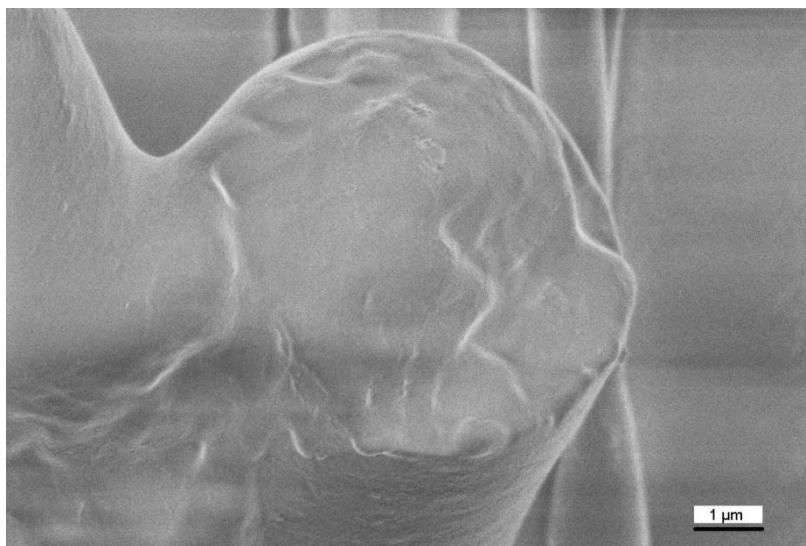Fig 7) Images of Iron ceramic composite made with Iron Nitrate, Urea, Ammonium Chloride. Note the veils. EDS confirms N, O, Fe and no C in these veils
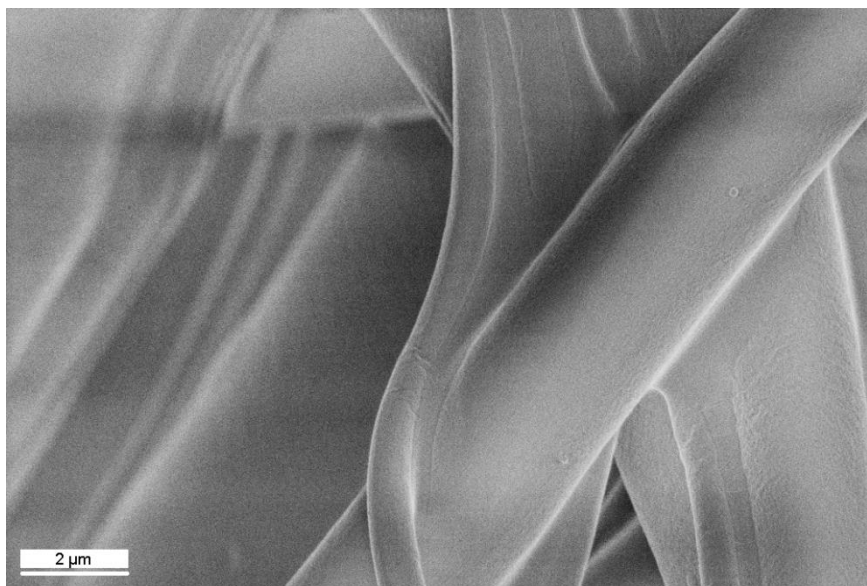
Fig 8) Nickel ceramic fibers. Made with Nickel Nitrate and Urea. Top
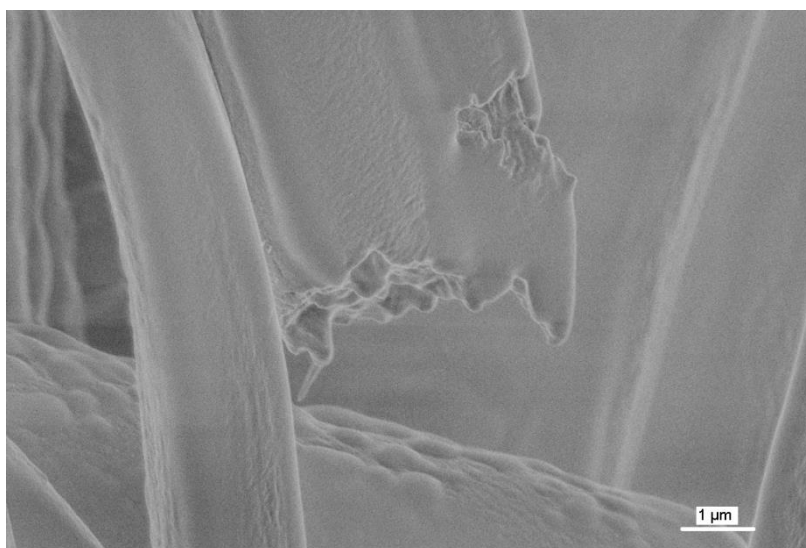
Fig 9) Zinc ceramic fibers [two images]. Made with Zinc Nitrate, Urea, Ammonium Chloride. Middle and bottom
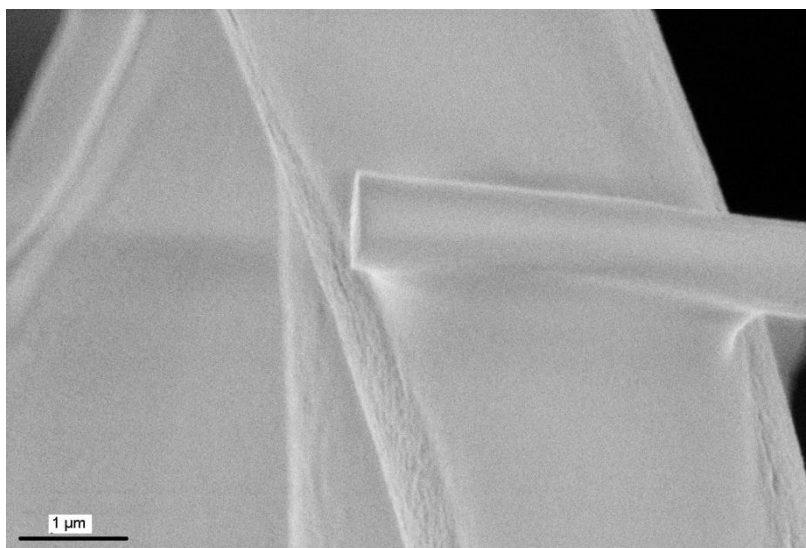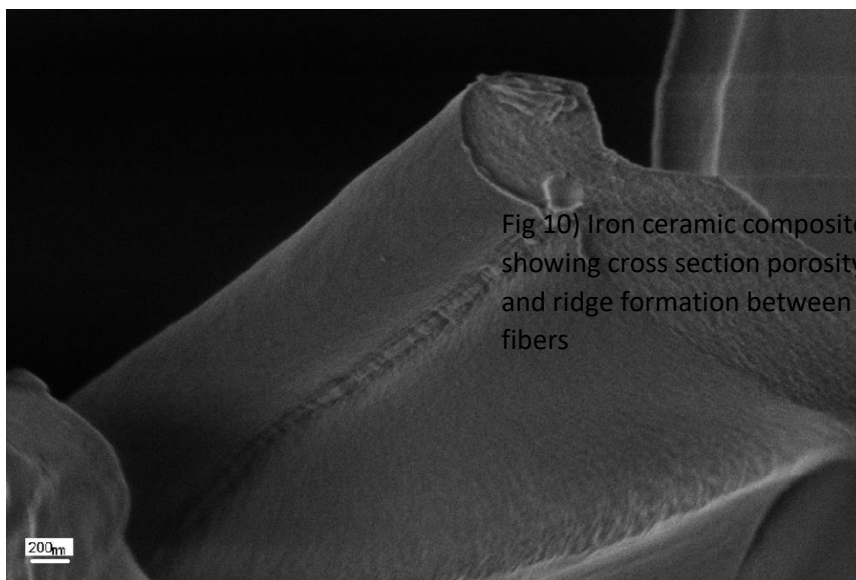
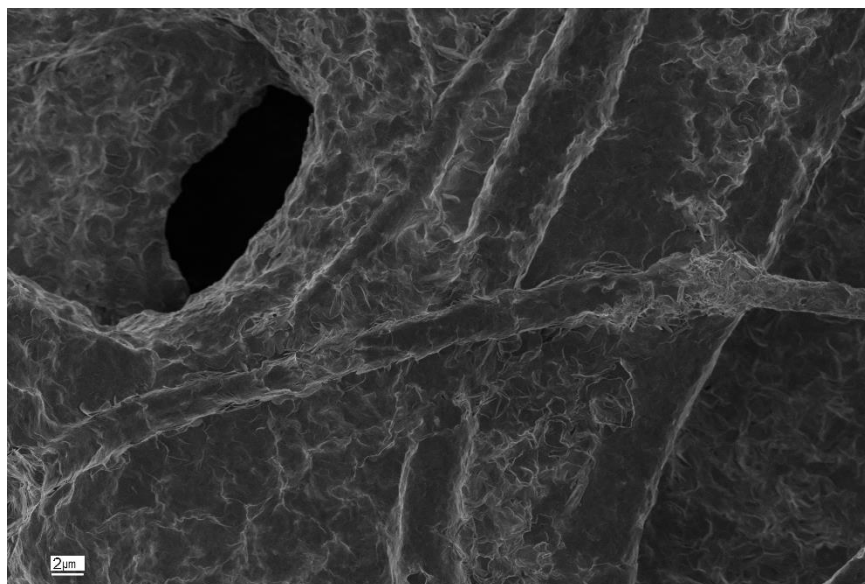Fig 10) Iron ceramic composite, showing cross section porosity and ridge formation between fibers

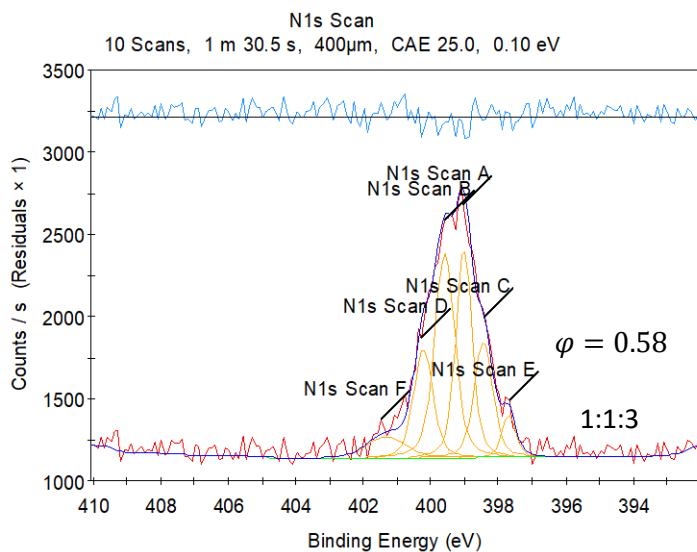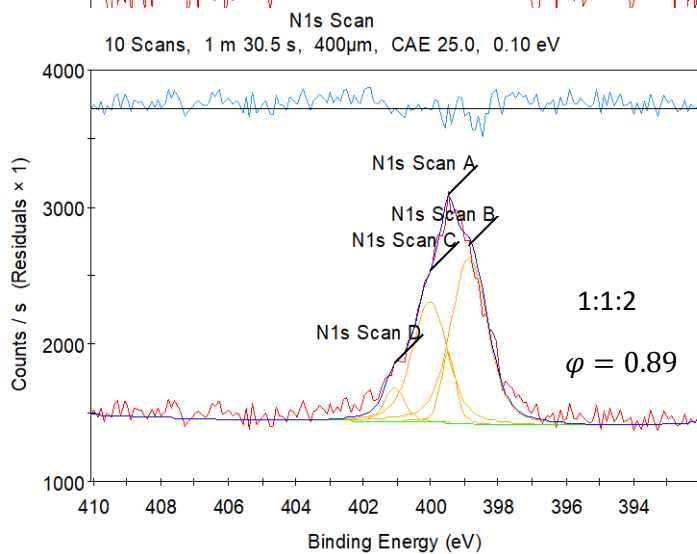Fig 11) Zinc Nitrate, Urea, Ammonium Chloride precursor dipped cellulose fibers

N1s Scan
10 Scans, 1 m 30.5 s, 400μm, CAE 25.0, 0.10 eV

N1s Scan A
N1s Scan B
1:1:1
$\varphi = 0.91$

N1s Scan
10 Scans, 1 m 30.5 s, 400μm, CAE 25.0, 0.10 eV

N1s Scan A
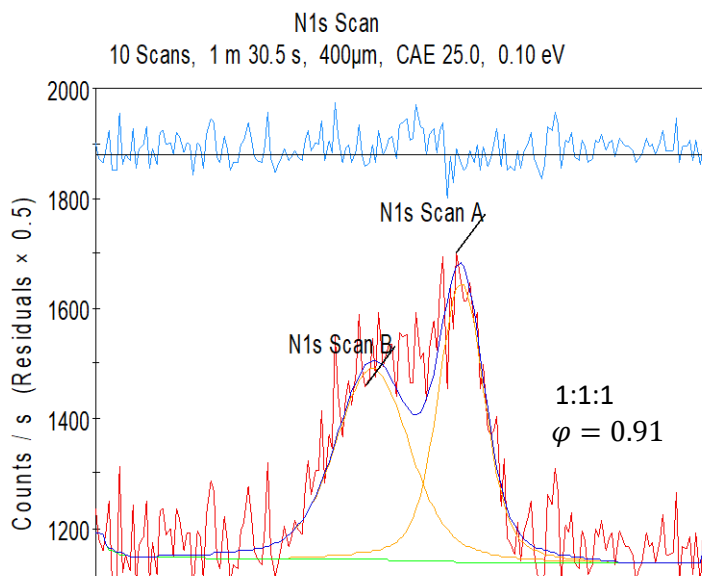N1s Scan B
N1s Scan C
N1s Scan D
1:1:2
$\varphi = 0.89$

Fig 12) N1s plots of XPS data for iron nitrate:acetylacetone:urea samples brought to different fuel-oxidizer profiles with nitric acid. The 1:1:3 material is the material reported here
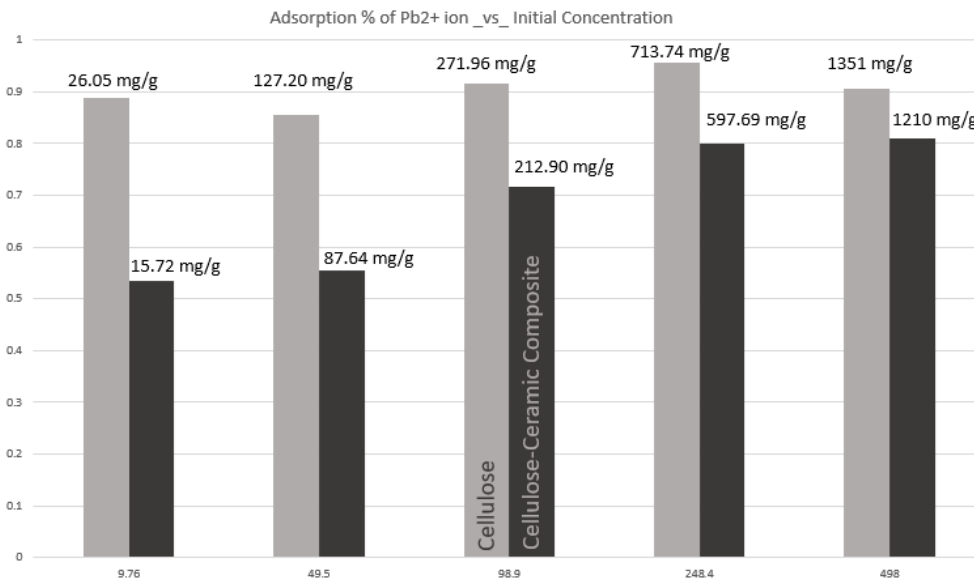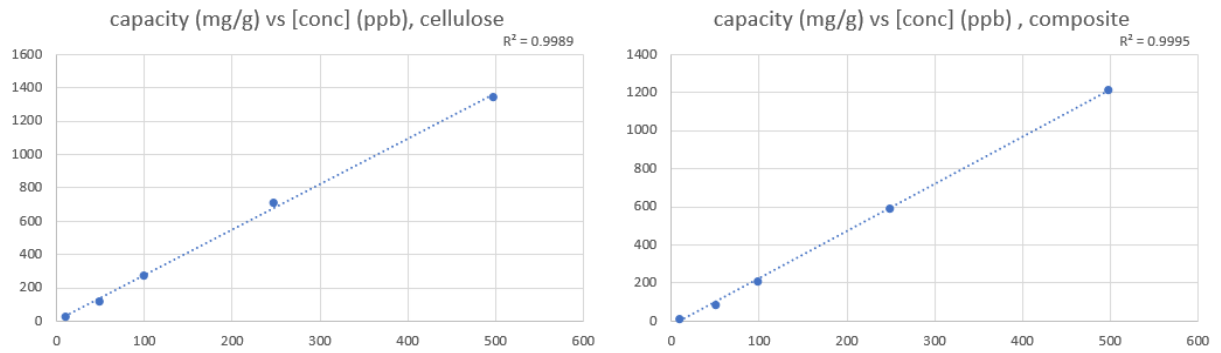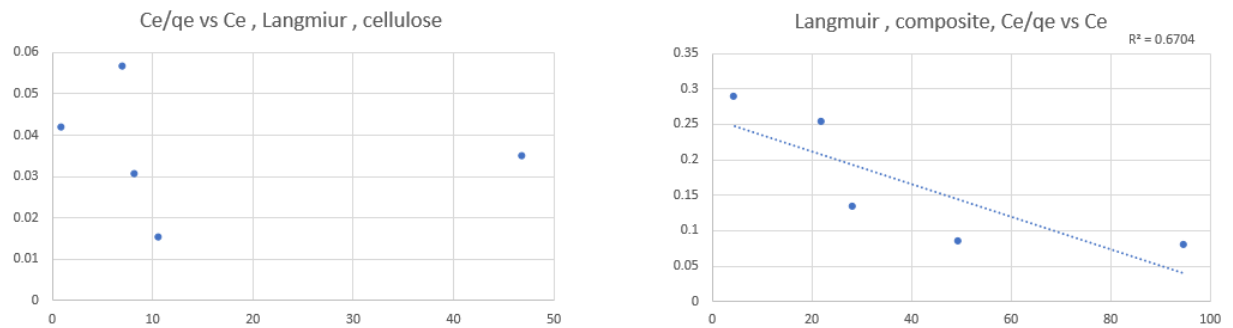
N1s Scan
10 Scans, 1 m 30.5 s, 400μm, CAE 25.0, 0.10 eV

N1s Scan A
N1s Scan B
N1s Scan C
N1s Scan D
N1s Scan E
N1s Scan F
$\varphi = 0.58$
1:1:3

Fig 13)

capacity (mg/g) vs [conc] (ppb), cellulose

R² = 0.9989

capacity (mg/g) vs [conc] (ppb) , composite

R² = 0.9995

Adsorption % of Pb2+ ion _vs_ Initial Concentration

26.05 mg/g   127.20 mg/g   271.96 mg/g   713.74 mg/g   1351 mg/g

597.69 mg/g

212.90 mg/g   1210 mg/g

15.72 mg/g   87.64 mg/g

Cellulose

Cellulose-Ceramic Composite

9.76   49.5   98.9   248.4   498

Fig 14)

Fig 15)

Ce/qe vs Ce , Langmiur , cellulose
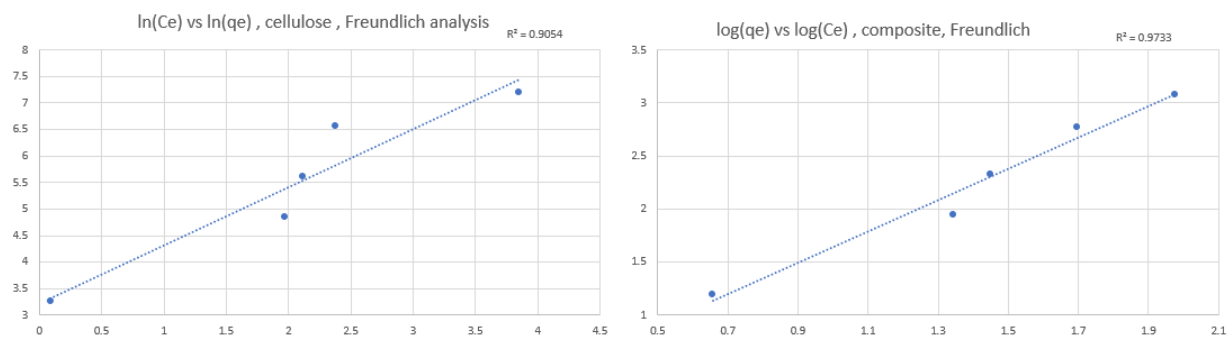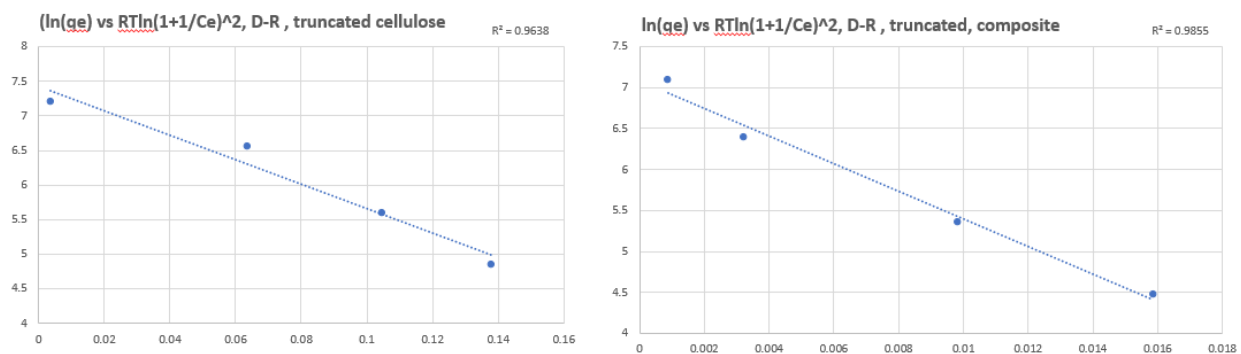
Langmuir , composite, Ce/qe vs Ce

R² = 0.6704

Fig 16)

Fig 17)

BIOGRAPHICAL SKETCH

Alejandro J. Castillo was born on the 16th of November, 1992 in the town of Harlingen, TX, to Isela and Frank Castillo. At the age of 17, he enrolled in the University of Texas Brownsville, and earned his associate of arts in general studies in 2011. With the merger of UTB and UTPA into the University of Texas Rio Grande Valley, he moved to the Edinburg campus, where he earned his Bachelor of Science in Physics and Chemistry in 2016. He entered the Lozano lab as a technician that summer. There, he operated a scanning electron microscope and formulated the research proposal which would become his thesis when he registered as a graduate student. He earned a Master of Science in Chemistry from the University of Texas Rio Grande Valley in August 2020.

To contact him, please send an email to alejandro.j.castillo011@gmail.com